AEROTHERMAL DATABASES AND CFD BASED LOAD PREDICTIONS

*M. Laureti *, S. Karl *, A. Marwege ** and A. Gülhan ***

* DLR Institute of Aerodynamics and Flow Technology
Bunsenstr. 10, 37073 Göttingen, Germany
mariasole.laureti@dlr.de - sebastian.karl@dlr.de

** DLR Institute of Aerodynamics and Flow Technology,
Supersonic and Hypersonic Technologies Department
Linder Höhe, 51147 Cologne, Germany
ansgar.marwege@dlr.de - ali.guelhan@dlr.de

ABSTRACT

The RETALT (Retro Propulsion Assisted Landing Technologies) project aims at investigating launch system reusability technologies for two different Vertical Take-off Vertical Landing launcher configurations, namely RETALT1 and RETALT2. This paper describes and summarizes the CFD based aerothermal load predictions, aerothermal database generation and application for the RETALT1 configuration for the complete trajectory. Furthermore, an analysis of representative CFD results is provided with the aim to show typical flow field phenomena and the resulting heating patterns occurring during the retro-propulsion phase. CFD results are then validated by comparison with the wind tunnel experiments carried out at different ground testing facilities in DLR Cologne.

Index Terms— Reusable Launch Vehicle, Retro-Propulsion, Aerothermal Loads, Wind Tunnel Experiments, CFD, RANS

Acronyms & Symbols

ACS	=	Aerodynamic Control Surfaces
ATDB	=	Aero-Thermal Data Base
CFD	=	Computational Fluid Dynamic
GTO	=	Geostationary Transfer Orbit
LEO	=	Low Earth Orbit
MECO	=	Main Engine Cut Off
RLV	=	Reusable Launch Vehicle
SSTO	=	Single Stage To Orbit
TPS	=	Thermal protection system
TSTO	=	Two Stage To Orbit
VTVL	=	Vertical Take-off Vertical Landing

M	=	Mach number
q	=	Heat flux per unit area (kW/m^2)
ρ	=	density (kg/m^3)
T	=	Temperature (K)
T_w	=	Wall temperature (K)
u	=	Velocity component along the launcher longitudinal axis (m/s)

1. INTRODUCTION

The Retro Propulsion Assisted Landing Technologies (RETALT) project, funded by the European Union Horizon 2020 program (grant agreement No 821890), has as objective to study critical technologies for Vertical Takeoff Vertical Landing (VTVL) Reusable Launch Vehicles (RLVs) applying retro propulsion combined with Aerodynamic Control Surfaces (ACS) [1]. Two reference launch vehicle configurations are defined:

- RETALT1: A heavy lift Two Stage To Orbit (TSTO) RLV with a payload of up to 14 t into the Geo Transfer Orbit (GTO). The first stage, the only one to be recovered, is powered by nine LOX/LH2 engines inspired to the Ariane' s Vulcain 2. The general layout of the RETALT1 configuration is similar to the SpaceX rocket "Falcon 9".

- RETALT2 A smaller Single Stage To Orbit (SSTO) configuration which is capable to deliver 500kg into Low Earth Orbits (LEO) similar to DC-X. The recovery of the full vehicle is foreseen.

The layout and system analysis of reusable launch vehicles include major challenges related to the application of a robust, light-weight, inexpensive and serviceable Thermal Protection System (TPS) [2]. The correct sizing of such a system, as well as other important structural parts like the aerodynamic control surfaces [3, 4, 5] and landing legs [6], relies on an accurate evaluation of thermal loads occurring during the entire atmospheric flight path [7].

The assessment of thermal loads, occurring on reusable launch vehicles during the entire trajectory, relies mainly on numerical simulations (CFD) due to the extremely high costs and limitations associated to extensive experimental campaigns on large-scale vehicles. On CFD side, the evaluation of the temperature distribution on the vehicle surface requires the coupling between such thermal load predictions and a structural response model. On the other hand the large disparity of fluid mechanical and structural time scales makes unsteady CFD analysis over the entire trajectory practically impossible, leading to the necessity to develop fast-response surrogate models for the aero-thermodynamic heating.

This paper describes the structure and construction of a surrogate aero-thermodynamic model, called Aero-Thermal Data Base (ATDB), which consists of a set of steady-state CFD results for the surface heat fluxes at different trajectory points, operational conditions of the engines and surface temperatures. The aero-thermal database created for the RETALT1 vehicle is based on a computational matrix that covers the entire flight trajectory in particular the flight regimes characterised by significant thermal loads or high dynamic pressure. In order to evaluate the heat flux on each point of the rocket surface as function of flight time and local surface temperature, interpolation algorithms are implemented. Finally the ATDB can be easily coupled to a structural response model to estimate the temperature history in each location on the vehicle surface during the entire trajectory.

The aim of this paper is also to analyse the results of representative CFD simulations, carried out for the aero-thermal data base construction, highlighting the presence of typical flow field phenomena occurring during the descent trajectory, with a focus on the re-entry burn, and the resulting heating pattern on the rocket structure. Interesting phenomena which affect the aero-thermodynamic heating of the vehicle surface are represented by the plume spreading, plume-to-plume interactions, immersion of the vehicle in hot exhaust gases and vehicle aerodynamics. Then the ATDB is coupled with a simple structural response model in order to prove the capability of this tool to estimate the temperature distribution on the overall rocket surface at any moment of the flight trajectory.

Finally, the numerical model used for CFD computations is validated by comparing the numerical results, obtained for a sub-scale model of the RETALT1, with the wind tunnel experiments performed by the DLR Department of Supersonic and Hypersonic Technologies in Cologne. Such experiments are part of an extensive experimental campaign whose aim is the simulation of the RETALT1 re-entry trajectory. The Hypersonic Wind Tunnel Cologne (H2K) is used for the re-entry burn simulations whereas the aerodynamic phase (without active engines) is studied by means of tests performed in the Trisonic Wind Tunnel Cologne (TMK). Finally, the Vertical Free-jet Facility Cologne (VMK) allows to investigate the exhaust plume occurring during the landing burn with cold gas experiments.

2. MATHEMATICAL & NUMERICAL MODEL

The heat flux data at different flight regimes and surface temperatures, used for the aero-thermal data base creation, are provided by an extensive CFD simulations campaign. These CFD analyses are performed with the hybrid structured-unstructured DLR Navier–Stokes solver TAU [8]. The TAU-code has been developed by the DLR Institute of Aerodynamics and Flow Technology and is a well established and widely used tool for a broad range of aerodynamic and aero-thermodynamic problems for both scientific and industrial applications. Furthermore the code is adapted for large-scale simulations on massively parallel computers. The TAU code is a second-order finite-volume flow solver for the Euler and Navier–Stokes equations in their integral forms, using eddy viscosity, Reynolds stress or detached and large eddy simulation for turbulence modelling.

The Spalart–Allmaras one-equation eddy viscosity model [9] has been employed for the present investigation. The choice is motivated by the robustness of such turbulence model along with the capability to reproduce the structure of engine exhaust-plumes during retro-propulsion maneuvers [5, 10]. The comparison between the experimental Schlieren pictures and numerical computations shows a very good agreement in the flow field representation as demonstrated in section 6.

Concerning the numerical scheme, the AUSMDV flux-vector splitting is applied together with MUSCL gradient reconstruction in order to achieve second-order spatial accuracy whilst maintaining a robust numerical treatment of strong discontinuities.

About mesh generation, TAU uses a cell-vertex finite volume discretization. The unstructured primary grid consists of tetrahedral, prismatic, pyramidal and hexahedral elements. Boundary layers are discretized with prismatic layers with a wall-normal stretching ratio of approximately 1.25. The dimensionless first wall spacing y+ is close to 1 as required by the Spalart-

Allmaras RANS model in its low-Reynolds formulation. The grid density is enhanced in regions of particular interest and large flow gradients (e.g. plumes and the near-base recirculation). Available flow symmetries are used. The CFD simulations for the RETALT1 flight configurations are performed by using half model for the ascent and a quarter-symmetry model for the descent. The hybrid/unstructured computational grids include approximately 7.7M grid points. Instead, for computations of the RETALT1 experimental model, the quarter-symmetry model is used only in presence of zero angle of attack, otherwise half model is adopted. The number of volumes is 5.5M and 11M respectively.

2.1. Thermodynamic model for the RETALT1 flight configuration

The thermodynamic model used for CFD simulations of RETALT1 flight configuration is based on a mixture of thermally perfect gases. The properties of the individual species are either computed from spectroscopic constants using partition functions that include an accurate representation of high temperature effects [11] or from NASA-Polynomials [12]. Appropriate mixture rules are applied to compute the thermodynamic properties depending on the local gas composition, pressure and density. For the computations a chemically frozen mixture of air ($76\,\%\,N_2$ and $24\,\%\,O_2$ by mass fraction) and engine exhaust gas ($97.7\,\%\,H_2O$, $2\,\%\,H_2$, $0.2\,\%\,OH$ and tracer species) is considered. The plume characteristics and exhaust gas composition at the RETALT1 nozzle exit have been obtained by a separate 2D-axisymmetric nozzle simulation where the flow is considered in chemical non-equilibrium and the Jachimowski reaction mechanism, described in Ref. [13], is employed. The resulting flow profiles, as well as the exhaust gas composition, are then prescribed as a Dirichlet inlet condition at the nozzle exit planes in the 3D simulations of the RETALT1 rocket [7].

The additional heat release due to post-combustion of the fuel-rich exhaust gases in the flow field around the rocket configuration is neglected. This assumption is justified by a preparatory study which shows that the frozen exhaust assumption yields realistic results for the surface heat flux [7]. Despite the error of the predicted gas temperatures increases with the free stream Mach number, the general plume and flow field structures are not affected.

2.2. Thermodynamic model for the RETALT1 experimental model

The CFD simulations of cold gas experiments on the RETALT1 scaled model are performed considering calorically perfect air as engine fluid. Separated 2D-axisymmetric nozzle simulation are carried out imposing total pressure and total temperature at the nozzle inlet. Also in this case, the resulting flow profiles are then prescribed as a Dirichlet inlet condition at the nozzle exit planes in the actual 3D simulations of the RETALT1 experimental model.

2.3. Structural response model

The aero-thermal database and associated interpolation algorithms provide the aero-thermodynamic heat flux on the rocket surface as function of time, location on the vehicle surface and wall temperature. The coupling of the ATDB to a structural response model allows to evaluate the temperature history during the entire flight path for in each position on the rocket surface.

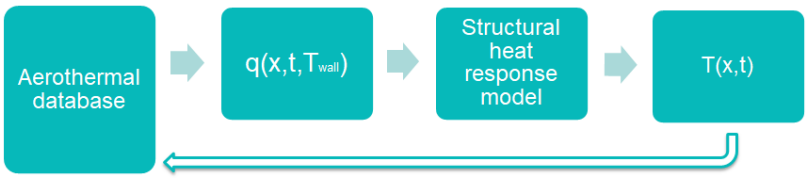

Fig. 1: ATDB coupling with the structural response model

An simple 0D structural response model is represented by the lumped mass method which describes the instantaneous heating of a chosen material characterized by thickness, δ, density, ρ and heat capacity, c. Starting from a temperature distribution $T\left(x,y,z,t_{old}\right)$, the new temperature distribution $T\left(x,y,z,t_{new}\right)$, evaluated at the time instant $t_{old}+\Delta t$, can be computed as follows:

$$T\left(x,y,z,t_{new}\right)=T\left(x,y,z,t_{old}\right)+\frac{q_c\left(x,y,z,t_{old}\right)-q_r\left(x,y,z,t_{old}\right)}{\rho c\delta}\Delta t \tag{1}$$

The temperature evolution is, therefore, driven by the difference of aero-thermodynamic heating, q_c, provided by the ATDB and conveniently interpolated, and the thermal radiation, q_r, divided by the product of the material properties. The thermal

radiation is given by Eq.2, where ϵ is the surface emissivity, σ is the Stefan–Boltzmann constant and T_{env} is the environment temperature.

$$q_r\left(x,y,z,t_{old}\right) = \sigma\epsilon\left(T\left(x,y,z,t_{old}\right)^4 - T_{env}^4\right) \tag{2}$$

3. DLR WIND TUNNEL FACILITIES AND RETALT1 EXPERIMENTAL MODEL

The experimental campaign carried out at DLR Department of Supersonic and Hypersonic Technologies in Cologne aims to investigate the RETALT1 re-entry trajectory. The retro-propulsion phase is studied in the Hypersonic Wind Tunnel Cologne (H2K) whereas the aerodynamic phase is tested in the Trisonic Wind Tunnel Cologne (TMK). The landing burn is studied by means experiments performed in the Vertical Free-jet Facility Cologne (VMK).

In this paper representative results of the H2K test series are shown and compared to CFD in order to validate the numerical model. A sketch of the Hypersonic Wind Tunnel Cologne is illustrated in Fig.2a. H2K is a blow down wind tunnel facility whose jet diameter measures 600 mm. The air passes through an electrical heater, a Laval nozzle, a test chamber, a diffuser and is ultimately released in a vacuum chamber. Several Mach numbers, i.e. 4.8, 5.3, 6.0, 7.0, 8.7 and 11.2 can be tested by using different nozzles. A wide range of Reynolds numbers can be achieved by changing the operative total pressure and total temperature. Quartz glass windows provide visual access to the test chamber for Schlieren imaging. A detail description of the H2K facility is provided in Ref. [14].

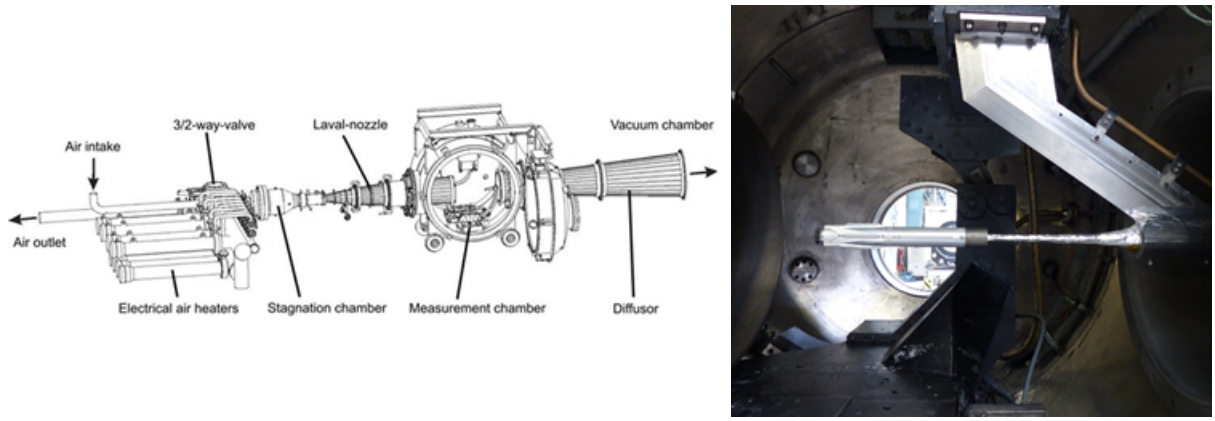

(a) H2K Cologne sketch

(b) RETALT1 model mounted in H2K

Fig. 2: Hypersonic Wind Tunnel Cologne (H2K) and RETALT1 experimental model

The RETALT1 model, mounted in the wind tunnel, is shown in Fig.2b. The model has a scaling of 1/130 compared to the RETALT reference configuration, it is equipped with high frequency pressure sensors meant for the detailed analyses of the base flow. For the simulation of the exhaust plume, air was blown out through a hollow model support string and a model Laval nozzle with an expansion ratio of 2.5. Various nozzle segments were manufactured for testing different engine combinations, i.e. one active engine or three active engines with different deflection angles.

4. RETALT1 MISSION AND CFD DATA SETS

This section aims to provide a description of the RETALT1 flight trajectory and the two re-entry scenarios for the RETALT1 first stage recovery, see sketch in Fig.3.

The ascent phase, from the take off until the Main Engine Cut Off (MECO), is attained by exploiting all the 9 LOX/LH2 engines of the first stage. This paper focuses on the analysis of the downrange-landing scenario as this imposes the design driving loads on the rocket configuration.

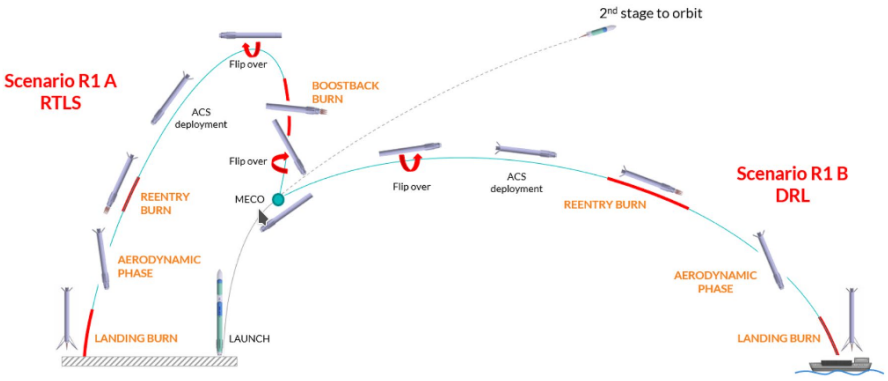

Fig. 3: Concept scenarios for the RETALT1 mission [15]

Right after MECO, the second stage main engine ignites and completes the injection of the payload to orbit. At this point, according to the defined mission, two possible scenarios for the first stage recovery are possible: for Geostationary Transfer Orbit (GTO) missions Down-range Landing (DRL) on a sea platform can be performed while for low earth orbit (LEO) missions, the first stage can accomplish a Return to Launch Site (RTLS), this scenario is not analysed in this paper because DRL imposes the highest heat loads.

For DRL scenario, the first stage continues the flight along a ballistic trajectory outside of the atmosphere, see Fig.4a. Before entry, the aerodynamic control surfaces are deployed and the vehicle is turned in a flip over maneuver. After entering the upper atmosphere (blue line) the re-entry burn, performed with 3 of 9 engines in operation, is initiated to reduce the flight speed (red line). This is followed by an aerodynamic unpropelled flight phase (green line), which is terminated by a landing burn, performed by using only the central engine, in order to ensure a controlled touch down (purple line). Thrust vector control (TVC) is used for low-speed maneuvering and the landing legs deploy shortly before touch-down. They include appropriate damping mechanisms which absorb the remaining kinetic energy.

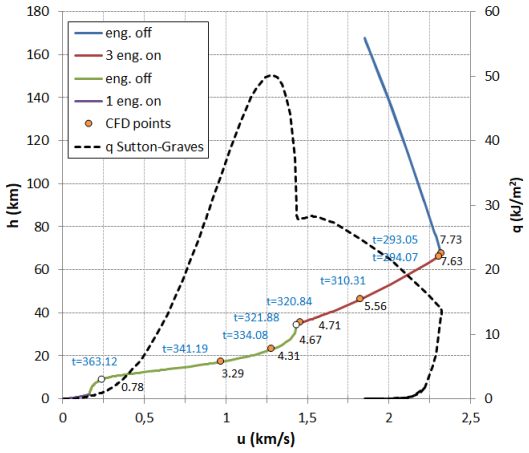

(a) Descent trajectory

#	Time (s)	h (km)	Mach
1	293,048	67,515	7,73
2	294,066	66,178	7,63
3	310,311	46,321	5,561
4	320,838	35,375	4,71
s5	321,857	34,419	4,665
5	334,084	22,962	4,313
6	341,195	17,187	3.291
s6	363.105	8,848	0,777

(b) Database population for descent configuration

Fig. 4: RETALT1 Descent trajectory points and flight conditions

In Fig.4a, the orange symbols indicate trajectory points for which CFD-analyses were performed (# 1-6) instead the white symbols (# s5-s6) indicate synthetic heat flux data computed by scaling the heat flux distribution in point # 5 and # 6 respectively. The scaling is performed by using well established general relationships between the global heat loads and the free stream properties [16, 17], and was only applied for trajectory points during the unpropelled flight phases. The use of a synthetic solution is justified when the fluid-dynamic conditions are not critical for the aero-thermal loads.
The dashed black line provides an estimation of the heat flux in the stagnation point downstream the bow shock and are obtained using the Sutton-Graves empirical equation [16]. Such equation is not able to provide meaningful results in the retro-propulsion

regime, due to the presence of the plume.

The free stream conditions in each CFD point for the descent trajectory are summarized in Fig.4b. The CFD computations are performed using fixed wall temperatures of 200K and 600K. This enables the database to account for the influence of the local wall temperature on the surface heat flux prediction. Since the flow field structures are not dramatically affected by the wall temperature, only results obtained for $T_w = 200$K are shown in this paper.

5. CFD REPRESENTATIVE RESULTS

Representative flow field solutions for the RETALT1 during the entry trajectory, and in particular, during the retro-propulsion phase, are shown in Fig. 5 and Fig.6.

The distribution of the pressure coefficient (left-hand side pictures) and surface heat flux (right-hand side pictures) are shown in color; Mach number and gas temperature in the symmetry plane are shown in gray-scale. In the left-hand side pictures, the brown iso-surface represents the boundary of 50% exhaust mass fraction and indicates the geometrical extend of the engine plumes. The streamlines are coloured by the longitudinal velocity component. In the right-hand side pictures, the brown iso-surface depicts the region of the flow field where $u = -100$ m/s in order to visualize the back flow.

5.0.1. Retro burn

The retro-burn begins when the vehicle is still at high altitude and high Mach, the free stream conditions in trajectory point # 2 are described in Tab.4b. Due to the low static free stream pressure, the plume significantly spreads downstream and upstream the vehicle which is totally immersed in a hot atmosphere made up by a large percentage of exhausted gas (see Fig.5a).

The streamlines indicate the presence of a large recirculation area surrounding the bottom part of the vehicle immediately downstream of the exhaust plume structure. The back flow is displayed by means of the brown iso-surface in Fig.5b, it redirects hot exhaust gases towards the base plate and spreads mainly in the transverse direction with respect to the axis in which the operative engines lay. The same picture shows the heat-flux distribution on the vehicle surface and the temperature field in the symmetry plane. Despite the hot gas surrounding the launcher the heat flux peaks remain low which is primarily due to the low density of the flow field: $q_{base\,plate} = 69$ kW/m^2 and $q_{planar\,fin} = 57$ kW/m^2.

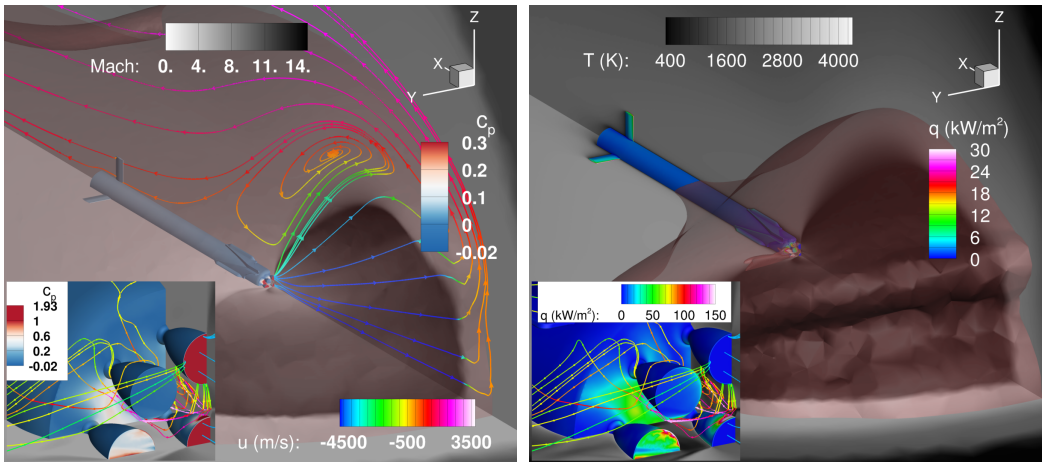

(a) Iso-surface of 50% exhaust mass fraction, Mach number, pressure coefficient

(b) Iso-surface of back flow, temperature, surface heat flux

Fig. 5: RETALT1 descent flow field structure (high altitude mode, h=66 km, Mach=7.6), beginning of retro propulsion

A flow field solution of particular interest is the one at the end of retro-propulsion due to the severe thermal loads occurring on the aerodynamic control surfaces which directly face the incoming flow being heated in the upstream stagnation zone (see Fig.6b). The heat flux here is the highest among the CFD points analysed, and can be regarded as the dimensioning value for the planar fins design. Free stream conditions are described in Tab.4b trajectory point # 4 and represent an example of mid-range altitude mode. Due to the moderate densities and the fact that the flow is aligned parallel to the vehicle surface, the heat fluxes on the central body remain moderate. The base plate heating during the retro-burn is not so intense due to the efficient shielding effect of the exhaust plume. The backflow region is significantly smaller compared to the beginning of retro-propulsion (high

altitude mode), here the brown iso-furface is confined in a limited area downstream the launcher and spreads slightly upstream the base plate.

An important reduction of the exhaust plume size can be observed in Fig.6a and is due to the increasing static and dynamic free stream pressure that occurs towards the end of the retro-burn. In this case only the lower part of the launcher is immersed in an atmosphere rich of hot exhausted gases.

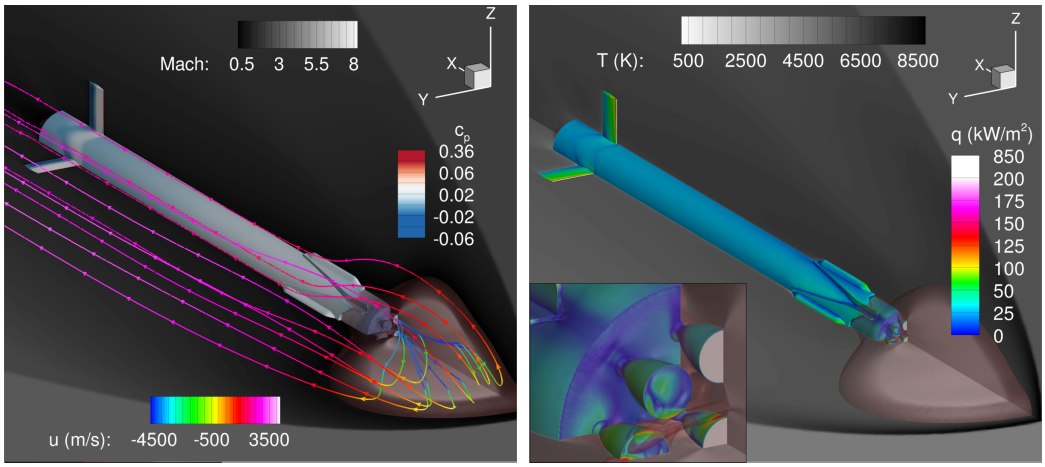

(a) Iso-surface of 50% exhaust mass fraction, Mach number, pressure coefficient

(b) Iso-surface of back flow, temperature, surface heat flux

Fig. 6: RETALT1 descent flow field structure (mid-range altitude mode, h=35km, Mach=4.7), end of retro propulsion

5.0.2. Time histories of heat loads

The time history of the average heat fluxes on the base plate and planar fin, during the descent trajectory, are shown in Fig.7. Considering the base plate (Fig.7a), it is possible to observe that the average heat flux remains approximately constant during retro-propulsion because of the exhaust plume shielding effect.

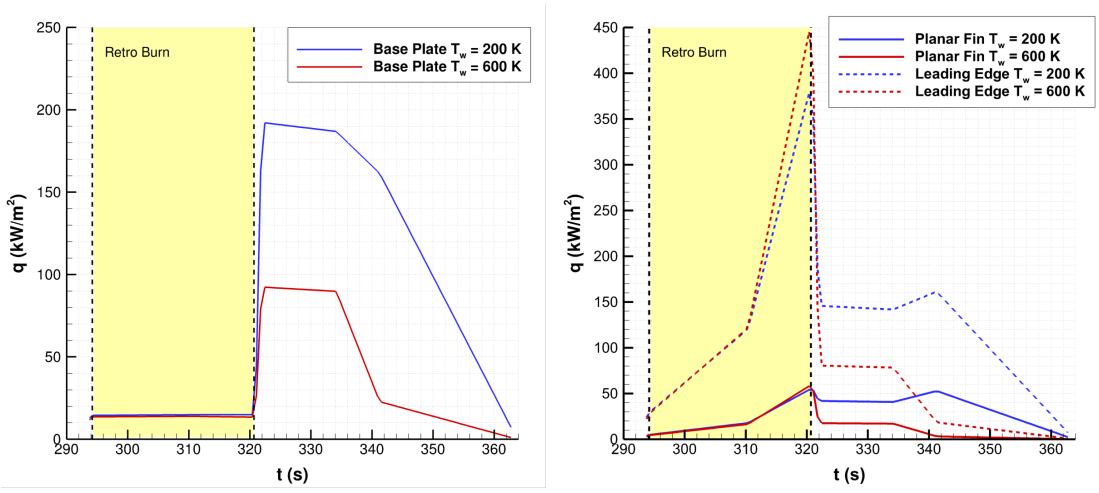

(a) Base plate

(b) Planar fin and leading edge

Fig. 7: RETALT1 time histories of average heat flux for constant wall temperatures - descent phase

Once the engines are turned off, the average heat flux goes through a sudden increase due to the presence of the bow shock and the associated aero-thermal heating close to the base plate. Between trajectory points #5s-5 the average heat flux slightly decreases, indeed in this part of the trajectory the flow conditions do not change significantly, and then rapidly declines due to

the strong reduction of the flight velocity.

Before discussing the averaged heat flux time evolution on a planar fin (Fig.7b), it is worth specifying that in these cases the averaging process provides information that needs to be read with caution. In fact, the heat flux on the planar fin reaches high values along the entire leading edge with a peak around the tip, elsewhere the heat flux is significantly lower. Because of the presence of strong local effects, the time histories of averaged heat flux on the leading edge are provided for both the wall temperatures (200K and 600K) and are represented by dashed lines.

Fig.7b shows that the averaged heat flux on the overall planar fin increases for the entire retro-propulsion duration due to the fact that the aerodynamic control surface directly face the incoming flow being heated in the upstream stagnation zone. Such increase of the average heat flux is also due to the larger flow density at lower altitude which leads to more confined plumes. After having reached the maximum value at the end of the retro burn the heat flux drops because the hot exhaust gases are blown away. The curves in Fig.7b exhibit a plateau between trajectory points #5s-5 then they show different trends depending on the wall temperature.

For $T_w = 600$K (red line) the average heat flux decreases because of the strong reduction in flight velocity. Concerning $T_w = 200$K (blue line) the average heat flux starts increasing again and reaches a local maximum. This effect is due to the heating provided by the surrounding atmosphere with the ambient temperature being larger than 200K.
The time histories of the averaged heat flux on the leading edge (dashed lines) follow the same qualitative trend of the overall fin, but levels are significantly higher ($\approx 86\%$ evaluated at the peak) proving that this region is the most critical in terms of thermal loads.

5.0.3. Aero-thermal database application

The detailed local heat flux data from the CFD analyses are organized in an aero-thermal database which, together with appropriate interpolation algorithms, can be easily coupled to a structural response model to evaluate the temperature history during the RETALT1 flight for each location on the vehicle surface, as shown in paragraph nr. 2.3. The material properties are summarized in Tab.1.

Table 1: Material properties used for the exemplary lumped-mass thermal analysis

Surface emissivity	ε	0.2	$(-)$
Wall thickness	δ	5	(mm)
Density	ρ	2600	(Kg/m^3)
Heat capacity	c	900	$(J/Kg/K)$

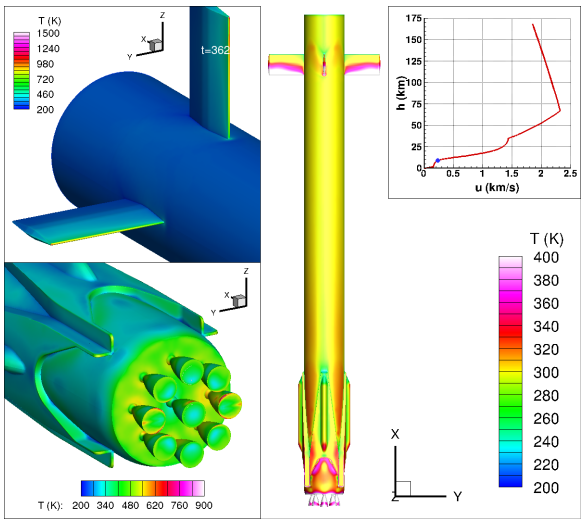

Fig. 8: RETALT1 surface temperature distribution close to the end of return trajectory

Fig.8 is made up of 4 frames: the trajectory point (top-right corner), the overall launcher (middle), planar fins (top-left

corner) and base plate/nozzles cluster (bottom-left corner). For every frame, a suitable contour scale is used.

The highest temperature occurs on the leading edge of the planar fin, close to the tip, with a peak of 1500K. Concerning the base plate, high temperatures are reached in the area enclosed by the engines cluster especially along Y-axis. During the retro-burn the external surfaces of the not operational engine's nozzles experience peak temperatures of 800K close to the exit plane. The central body, from the the folded legs up to the top, is characterized by an average temperature of 300K, higher values can be found in the bottom part of the launcher.

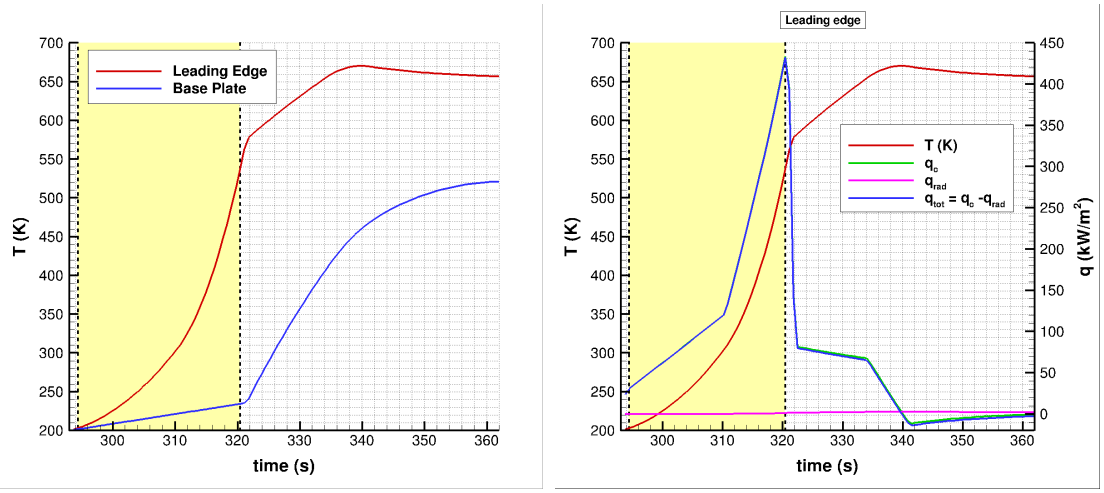

(a) Time history of the average temperature on the planar fin leading edge and base plate

(b) Time history of the heat fluxes on the planar fin leading edge

Fig. 9: Average temperature time evolution

The time evolution of the average temperature on the planar fin leading edge and on the base plate is shown in Fig.9a. About the base plate, it is possible to observe that the rate of increase of the average temperature is rather low during the retro-propulsion phase because of the plume shielding effect. In accordance with Fig.7a, the following sudden temperature increase, during the aerodynamic phase, is due to aero-thermal heating provided by the bow shock located close the base plate.

Concerning the planar fin, the average temperature increases with an high rate during the retro-burn due to direct exposure of the control surface to the incoming hot flow. At the end of retro-propulsion, the average temperature keeps increasing but the curve slope decreases significantly. The reason lies in the drop of the total heat flux which essentially corresponds to the aero-thermodynamic heating, in fact thermal radiation provides a very low contribution, see Fig.9b. This picture shows also that the total heat flux crosses the zero at around t=340 s and then becomes negative. This happens because the aerodynamic control surface is warmer than the surrounding atmosphere and the vehicle Mach number is decreasing. When the total heat flux is zero, the average temperature exhibits a maximum and then starts slowly decreasing.

6. WIND TUNNEL EXPERIMENTS

In this section a comparison between some CFD results and Hypersonic Wind Tunnel Cologne (H2K) tests are compared. H2K facility, in fact, has been used for carrying out an extensive campaign of experiments with the aim to investigate the RETALT1 re-entry burn. A detailed description of the RETALT1 experimental model and configurations can be found in Ref.[5].

The experiments are performed using a nominal Mach number of 5.29, the free-stream stagnation conditions, p0 and T0, as well as the engine total pressure and total temperature, pCC and TCC, are summarized in Tab.2.

Table 2: Experimental test matrix

Computations	Model	Run	Engines	Alpha DSC [°]	Configuration	Mach	p0 [bar]	T0 [K]	pCC [bar]	TCC [K]
1	Short	76	0	0	I	5.29	4	450	0	300
2	Short	81, 90	1	0	I	5.29	4	450	20	300
3	Short	84, 92	1	10	I	5.29	4	450	20	300
4	Short	93	3	0	I	5.29	4	450	12.3	300
4	Short	101	3	0	--	5.29	4	450	12.3	300
5	Short	96	3	10	I	5.29	4	450	12.3	300
6	Short	107	3	10	--	5.29	4	450	12.3	300

Fig.10a shows a comparison between the Schlieren pictures obtained by CFD simulation and wind tunnel measurements for the case with one operative engine (the central one) and angle of attack $AoA = 0°$. The bow shock, in the numerical result, is located slightly farther away from the body than in the experiment and small differences in plume shape can be observed. The flow structure in the plume region is complex due to the incoming hypersonic flow that encounters the jet flow from the engine. Just downstream of the bow shock wave it is possible to observe the mixing region where the free stream air is mixed with the jet coming out of the engine. Since the gases have different densities, the mixing region is characterized by a density gradient. Finally, a Mach disk is formed at the end of the plume. Between the Mach disk and the mixing surface there is a subsonic region.

The pressure, measured by high frequency sensors located on the surface of the RETALT1 experimental model, is then compared to the numerical one. Sensors 11-12-13-14 are placed at beginning of the cylindrical region, 21-22-23-24 are positioned slight upstream the folded legs, 313 and 333 are placed in the region that connects the base plate to the bottom part of the cylindrical body, 312-322-332-342 are on the base plate around the engines cluster and finally 311 and 331 are located close to the central engine. Fig. 10b show that numerical pressure is slightly lower than the experimental one except for sensor 313 where it is higher. The percentage error is below 10% for most of the sensors, instead, for sensors 342 and 312, it takes the values of 18% and 24%, respectively. These data show that there is a very good agreement between the pressure experimentally measured and the pressure computed via CFD despite the extremely complicated flow field which develops close to the base plate due to the plume-plume interactions.

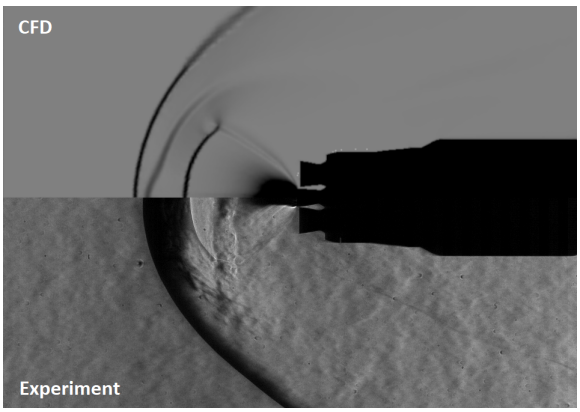

(a) Schlieren pictures comparison: CFD (top) vs. experimental (bottom).

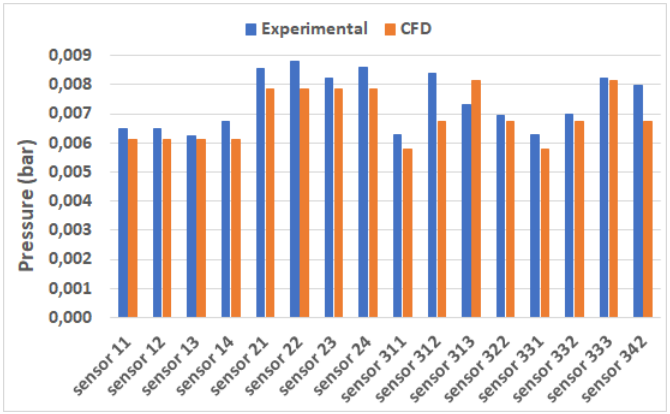

(b) Surface pressure comparison

Fig. 10: Test 2: active central engine, $AoA = 0°$.

The experiments with 3 operative engines active showed some wavy patterns which indicate the presence of flow unsteadiness. Such unsteady behaviour is remarkable in the case with $AoA = 0°$ whereas is less accentuated when the angle of attack is equal to $10°$. Although the unsteadiness level is lower in the the latter case, a wavy pattern can be noticed downstream the bow shock, see Fig.11b. In the case with $AoA = 10°$ the amplitude of the bow shock oscillations is not so large and this justify the possibility of comparing a single Schlieren snapshot to the numerical flow field, see Fig.11a. The presence of an angle of attack different from zero has a stabilizing effect on the flow field and makes the plume asymmetric.

The superposition of the numerical Mach field and the experimental Schlieren picture, represented in Fig.11a, shows that the central structure of the plume is well represented by the CFD simulation instead the Mach disk is more distant from the body compared to the experimental result. Same considerations apply for the bow shock except for the region below the vehicle where a good agreement between the experimental result and the numerical one can be observed.

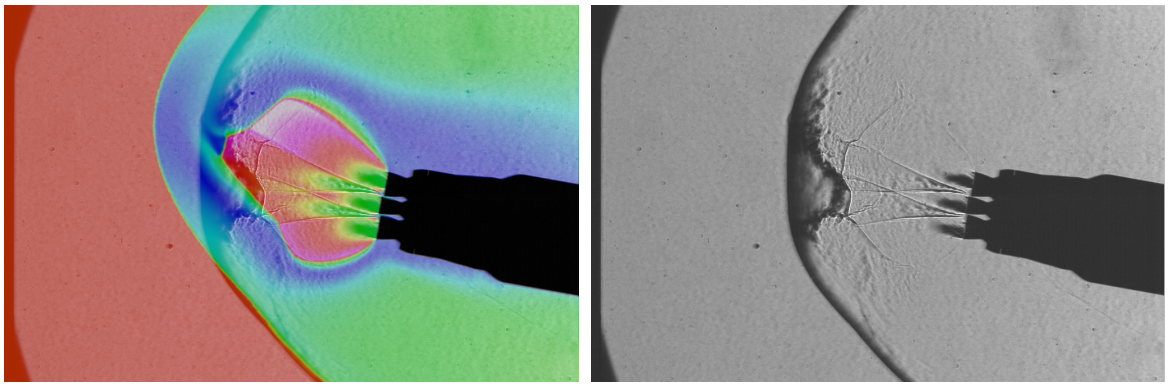

(a) CFD Mach coloured contour superimposed to the experimental Schlieren picture

(b) Experimental Schlieren picture

Fig. 11: CFD simulation vs. experimental Schlieren, Test 5: 3 operative engines, $AoA = 10°$.

7. CONCLUSIONS

A fast-response surrogate model for the aero-thermodynamic heating of the RETALT1 launcher, during both the ascent flight and the atmospheric entry, was created. This model is based on an aero-thermal database (ATDB) consisting in a large set of steady-state CFD results for the surface heat fluxes for different flight regimes and surface temperatures. Interpolation algorithms allow the estimation of heat loads as a function of the flight time and local surface temperatures. The computational matrix covered the entire RETALT1 flight trajectory. CFD simulations were performed mainly around peak heating and at critical flight conditions whereas scaling laws are used to evaluate thermal loads in aerodynamic flight conditions characterized by low heating rates. The coupling of the ATDB to a structural response model allows to estimate the temperature history in each location on the vehicle surface during the entire trajectory.

The paper focused on the analysis on the downrange-landing scenario, and in particular on the retro-propulsion phase, since it imposes the design driving loads on the rocket configuration. Representative flow field solutions and typical phenomena, occurring for high altitude and low altitude flow modes, were analysed. At high altitudes the ambient pressure is low and the plumes significantly spread out resulting in strong plume-plume interaction. The vehicle is fully immersed in a hot exhausted gases atmosphere but, thanks to the low flow field density, the heat loads on the rocket surface are limited. At lower altitudes, where the atmospheric pressure is larger, the exhaust plumes are confined and the intensity of plume-plume interactions on the launcher base plate are less significant. The flow field conditions at the end of the retro burn provide the most critical thermal load on the leading edge of the planar fin which directly face the incoming flow being heated in the upstream stagnation zone.

The ATDB, along with the interpolation algorithms, was then coupled with a simple structural response model to show the capability of such tool to compute the temperature time evolution on the rocket surface. In particular the time history of the average temperature on the base plate and ACS leading edge was analysed. These components were chosen as representative examples because they experience the most critical thermal loads.

The comparison of CFD calculations with Schlieren pictures from the experiment showed small differences in the bow shock stand-off distance for the case with the central engine active. Larger discrepancies can be observed in the case with 3 operative engines, nevertheless the central structure of the plume is well represented. It is important to highlight that despite the differences between the experimental results and the numerical ones, in terms of the flow field representation, CFD pressure matches very well the measured one for most of the experiments.

In conclusion, the general good agreement between experimental results and CFD computations proves that the selected numerical model and set-up, as well as the meshing criterion, are capable to represent the physical phenomenology of retro propulsion. Such validation justify the use of the same methodology even for the RETALT1 flight configuration.

8. ACKNOWLEDGEMENTS

This project has received funding from the European Union's Horizon 2020 research and innovation framework program under grant agreement No 821890. We gratefully acknowledge the interest in our work and the opportunity to forward this essential research.

9. REFERENCES

[1] A. Marwege, A. Gülhan, J. Klevanski, J. Riehmer, D. Kirchheck, S. Karl, D. Bonetti, J. Vos, M. Jevons, A. Krammer, and J. Carvalho, "Retro propulsion assisted landing technologies (retalt): Current status and outlook of the eu funded project on reusable launch vehicles," *70th International Astronautical Congress (IAC), Washington D.C., United States*, 2019.

[2] S. Paixão, C. Peixoto, M. Reinas, and J. Carvalho, "Retalt tps design and manufacturing," *CEAS Space Journal, https://doi.org/10.1007/s12567-021-00417-w*, 2022.

[3] D. Charbonnier, J. Vos, A. Marwege, and C. Hantz, "Computational fluid dynamics investigations of aerodynamic control surfaces of a vertical landing configurations," *CEAS Space Journal, doi:10.1007/s12567-022-00431-6*, 2022.

[4] A. Marwege, C. Hantz, D. Kirchheck, J. Klevanski, A. Gülhan, D. Charbonnier, and J. Vos, "Wind tunnel experiments of interstage segments used for aerodynamic control of retro-propulsion assisted landing vehicles," *CEAS Space Journal, https://doi.org/10.1007/s12567-022-00425-4*, 2022.

[5] J. Vos, D. Charbonnier, A. Marwege, A. Gülhan, M. Laureti, and S. Karl, "Aerodynamic investigations of a vertical landing launcher configuration by means of computational fluid dynamics and wind tunnel tests," *AIAA SCITECH 2022 Forum, https://doi.org/10.2514/6.2022-1308*, San Diego, 2022.

[6] A. Krammer, L. Blecha, and M. Lichtenberger, "Fin actuation, thrust vector control and landing leg mechanisms design for the retalt vtvl launcher," *CEAS Space Journal, https://doi.org/10.1007/s12567-021-00421-0*, 2022.

[7] M. Laureti and S. Karl, "Aerothermal databases and load predictions for retro propulsion assisted launch vehicles (retalt)," *CEAS Space Journal, https://doi.org/10.1007/s12567-021-00413-0*, 2022.

[8] S. Langer, S. Schwöppe, and N. Kroll, "The dlr flow solver tau—status and recent algorithmic developments," *AIAA Paper 2014-0080*, 2014.

[9] P.R Spalart and S.R Allmaras, "A one-equation turbulence model for aerodynamic flows," *AIAA Paper 1992-0439*, 1992.

[10] T. Ecker, S. Karl, E. Dumont, S. Stappert, and D. Krause, "Numerical study on the thermal loads during a supersonic rocket retropropulsion maneuver," *Journal of Spacecraft and Rockets 57(1) 131-146*, 2020.

[11] B. Bottin, "Aerothermodynamic model of an inductively-coupled plasma wind tunnel," *PhD-Thesis, University of Liege*, 1999.

[12] S. Gordon and B. J. McBride, "Computer program for calculation of complex chemical equilibrium compositions and applications," *NASA Reference Publication 1311*, 1994.

[13] P. Gerlinger, "An implicit multigrid method for turbulent combustion," *Journal of Computational Physics, Vol. 167: 247-276*, 2001.

[14] F.J. Niezgodka, "Der hyperschallwindkanal h2k des dlr in köln-porz (stand 2000)," *DLR-Mitt. 2001-01, Cologne.DOI: 10.13009/ EUCASS2017-680*, 2001.

[15] G. De Zaiacomo, G.B. Arnao, R. Bunt, and D. Bonetti, "Mission engineering for the retalt vtvl launcher," *CEAS Space Journal, https://doi.org/10.1007/s12567-021-00415-y*, 2022.

[16] K. Sutton and R.A. Graves, "A general stagnation point convective heating equation for arbitrary gas mixtures," *NASA TR-R-376*, 1971.

[17] G.T. Chapman, "Theoretical laminar convective heat transfer and boundary layer characteristics on cones at speeds to 24 km/s," *NASA TN D-2463*, 1964.